Supplementary of

Vertical distribution of atmospheric particulate matters within urban boundary layer in southern China: size-segregated chemical composition and secondary formation through cloud processing and heterogeneous reactions

Shengzhen Zhou[1,8*], Luolin Wu[1], Junchen Guo[1], Weihua Chen[2], Xuemei Wang[2*], Jun Zhao[1], Yafang Cheng[2,7], Zuzhao Huang[3], Jinpu Zhang[4], Yele Sun[5], Pingqing Fu[6], Shiguo Jia[1], Yanning Chen[4], Junxia Kuang[4]

[1] School of Atmospheric Sciences, and Guangdong Province Key Laboratory for Climate Change and Natural Disaster Studies, Sun Yat-sen University, Guangzhou, 510275, P. R. China

[2] Institute for Environmental and Climate Research, Jinan University, Guangzhou, 511443, P. R. China

[3] Guangzhou Environmental Technology Center, Guangzhou, 510180, P. R. China

[4] Guangzhou Environmental Monitoring Center, Guangzhou, 510030, P. R. China

[5] State Key Laboratory of Atmospheric Boundary Layer Physics and Atmospheric Chemistry, Institute of Atmospheric Physics, Chinese Academy of Sciences, Beijing, 100029, P. R. China

[6] Institute of Surface-Earth System Science, Tianjin University, Tianjin, 300072, P. R. China

[7] Multiphase Chemistry Department, Max Planck Institute for Chemistry, P.O. Box 3060, Mainz, 55128, Germany.

[8] Southern Laboratory of Ocean Science and Engineering (Guangdong, Zhuhai), 519082, P. R. China

Correspondence to: Shengzhen Zhou (zhoushzh3@mail.sysu.edu.cn) and Xuemei Wang (eeswxm@mail.sysu.edu.cn)

1. PMF model

A positive matrix factorization (PMF) model was used to resolve mass size distribution modes. PMF is a commonly used multivariate factor analysis technique that is capable of decomposing the aerosol chemical species data matrix into two matrices, factor profiles and factor contributions:

$$x_{ij} = \sum_{k=1}^{p} g_{ik} f_{kj} + e_{ij} \quad (1)$$

and

$$Q = \sum_{i=1}^{n} \sum_{j=I}^{m} \left[\frac{x_{ij} - \sum_{k=1}^{p} g_{ik} f_{kj}}{u_{ij}} \right]^2 \quad (2)$$

where the element x_{ij} is the concentration value of the *i*th sample at the *j*th size interval or species; g_{ik} is the amount of mass contributed from the *k*th source associated with the *i*th sample and f_{kj} is the size distribution or species profile associated with the *k*th source; e_{ij} is the residual for each sample or species. The aim of the PMF solution is to minimize the object function Q (Eq. (2)) via a conjugate gradient algorithm, based upon estimated data uncertainties (or adjusted data uncertainties) u_{ij} (Brown et al., 2015). In this work, the EPA PMF 5.0 software package was used to perform the calculation (Norris et al., 2014). The uncertainties for the observed data were prepared based on the recommended method in the EPA PMF 5.0 manual. PMF was proved to be an efficient method to resolve overlapped modes of particle size distribution in early works (Guo et al, 2010; Liu et al, 2015). Totally 540 sets (30 samples × 6 species × 3 levels) of mass size distribution data were generated at the 3 heights (the ground level, 118 m, and 488 m) of Canton Tower. Six species include K^+, NH_4^+, SO_4^{2-}, Cl^-, Na^+, and NO_3^- at each height respectively. PMF analysis was executed on these 540 sets of data. At last, 3 factors implying 3 modes marked by their peaks were chosen to obtain the most reasonable solution.

The following figure shows the 3 PMF resolved size distribution modes fitted by lognormal function through Matlab software to determine mass medium aerodynamic diameters (MMAD) and eventually explaining 94% of total measured aerosol mass. The MMAD in this work was 0.33, 0.75, 4.6 μm corresponding condensation mode, droplet mode and coarse mode respectively, which presented a remarkable similarity to former urban aerosol research in Hong Kong (Gao et al. 2016). PMF resolved average particle concentrations for each mode at ground level, 118 m, and 488 m during autumn and winter campaigns were showed in **Table S1.**

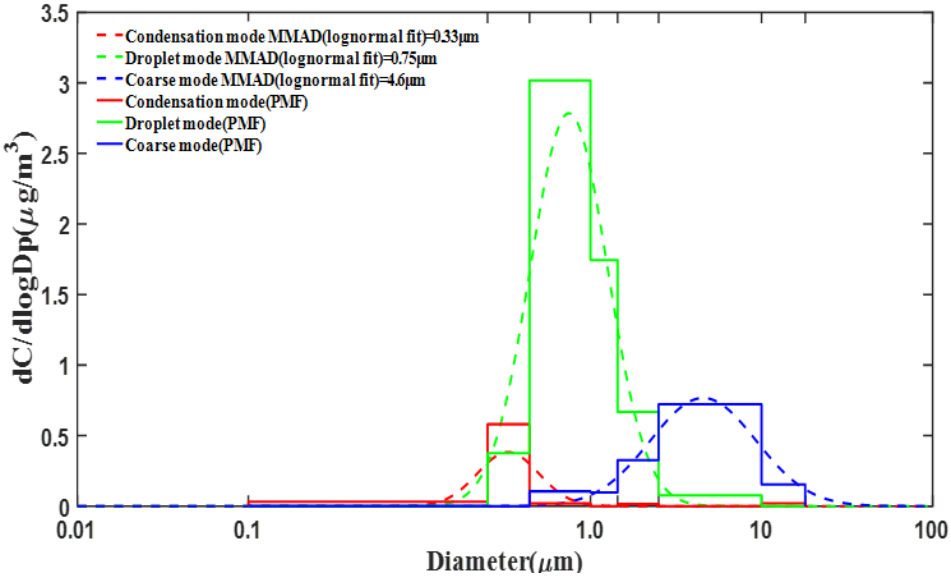

Three modes resolved by PMF

References:

Brown, S. G., Eberly, S., Paatero, P., and Norris, G. A.: Methods for estimating uncertainty in PMF solutions: Examples with ambient air and water quality data and guidance on reporting PMF results, Sci. Total Environ., 518, 626-635, http://dx.doi.org/10.1016/j.scitotenv.2015.01.022, 2015.

Gao, Y., Lee, S. C., Huang, Y., Chow, J. C., and Watson, J. G.: Chemical Characterization and Source Apportionment of Size-Resolved Particles in Hong Kong Sub-Urban Area, Atmospheric Research, 170, 112-22, http://dx.doi.org/10.1016/j.atmosres.2015.11.015, 2016.

Guo, S., Hu, M., Wang, Z., Slanina, J., and Zhao, Y.: Size-resolved aerosol water-soluble ionic compositions in the summer of Beijing: implication of regional secondary formation. Atmos. Chem. Phys. 10, 947-959, https://doi.org/10.5194/acp-10-947-2010, 2010.

Liu, Z., Xie, Y.Z., Hu, B., Wen, T. X., Xin, J.Y., Li, X. R., and Wang, Y. S.: Size-resolved aerosol water-soluble ions during the summer and winter seasons in Beijing: Formation mechanisms of secondary inorganic, Chemosphere, 183, 119-131, http://dx.doi.org/10.1016/j.chemosphere.2017.05.095, 2017.

Norris, G., Duvall, R., Brown, S., and Bai, S.: EPA Positive Matrix Factorization (PMF) 5.0 fundamentals and User Guide Prepared for the US Environmental Protection Agency Office of Research and Development, Washington, DC., 2014.

Table S1. PMF resolved average particle concentrations for each mode at ground level, 118 m and 488 m during autumn and winter campaigns.

		Condensation mode (μg/m^3)		**Droplet mode (μg/m^3)**		**Coarse mode (μg/m^3)**	
		autumn	winter	autumn	winter	autumn	winter
K^+	ground	0.05±0.03	0.11±0.07	0.21±0.09	0.39±0.35	0.05±0.02	0.04±0.03
	118m	0.05±0.03	0.12±0.09	0.18±0.08	0.37±0.31	0.06±0.02	0.04±0.03
	488m	0.03±0.01	0.04±0.03	0.15±0.07	0.2±0.17	0.03±0.01	0.03±0.02
NH_4^+	ground	0.2±0.15	0.46±0.22	1.21±0.78	2.64±2.34	0.05±0.07	0.14±0.22
	118m	0.24±0.21	0.48±0.27	1.4±0.9	2.23±2.52	0.12±0.12	0.15±0.22
	488m	0.07±0.08	0.38±0.13	1.63±0.78	1.85±2.01	0.12±0.09	0.19±0.23
SO_4^{2-}	ground	0.53±0.43	0.95±0.43	4.23±2.26	6.45±4.06	0.57±0.25	0.82±0.83
	118m	0.59±0.49	0.99±0.49	4.45±2.32	6.2±3.9	0.63±0.28	0.68±0.83
	488m	0.25±0.17	0.71±0.25	4.52±2.17	5.26±4.64	0.43±0.24	0.57±0.53
Cl^-	ground	0.03±0.1	0.03±0.03	0.12±0.21	0.94±1.6	0.52±0.47	0.35±0.39
	118m	0.03±0.11	0.05±0.06	0.06±0.1	1.1±1.82	0.72±0.68	0.31±0.35
	488m	0±0.01	0.01±0.02	0.08±0.08	0.22±0.31	0.31±0.22	0.2±0.35
Na^+	ground	0.03±0.01	0.03±0.04	0.06±0.04	0.12±0.11	0.52±0.44	0.12±0.18
	118m	0.04±0.02	0.04±0.04	0.01±0.01	0.12±0.11	0.61±0.53	0.11±0.15
	488m	0.01±0.01	0.01±0.02	0.04±0.05	0.07±0.05	0.45±0.33	0.11±0.23
NO_3^-	ground	0.09±0.08	0.43±0.33	0.46±0.44	5.93±7.9	2.39±1.39	1.46±1.43
	118m	0.15±0.12	0.45±0.31	0.88±0.87	6.53±8.34	2.99±1.87	1.34±1.69
	488m	0.07±0.09	0.16±0.17	0.74±0.85	3.28±3.53	2.25±1.34	1.4±1.41

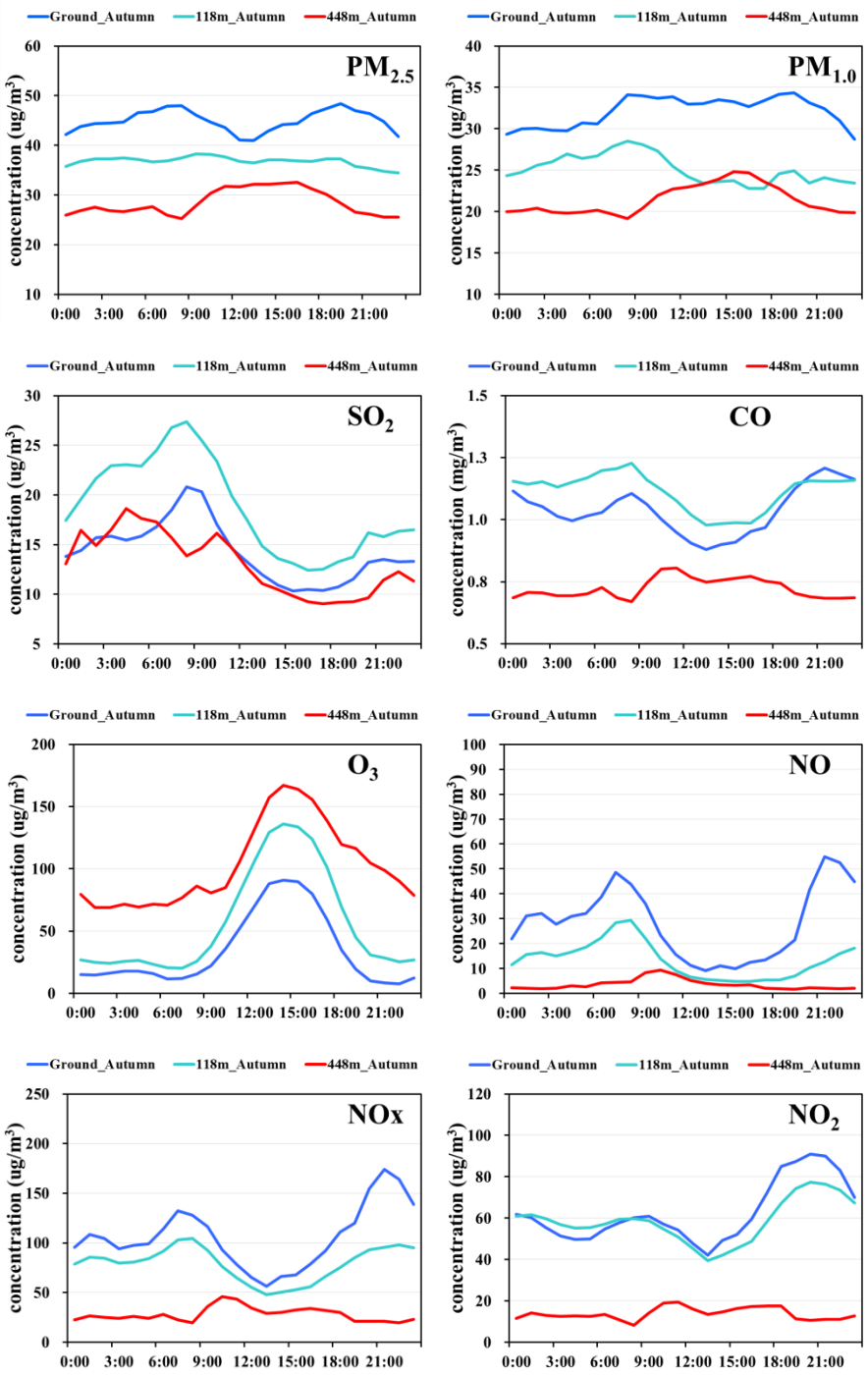

Figure S1. Diurnal variations of concentrations of pollutants at different altitudes on the Canton Tower during the autumn field stuty.

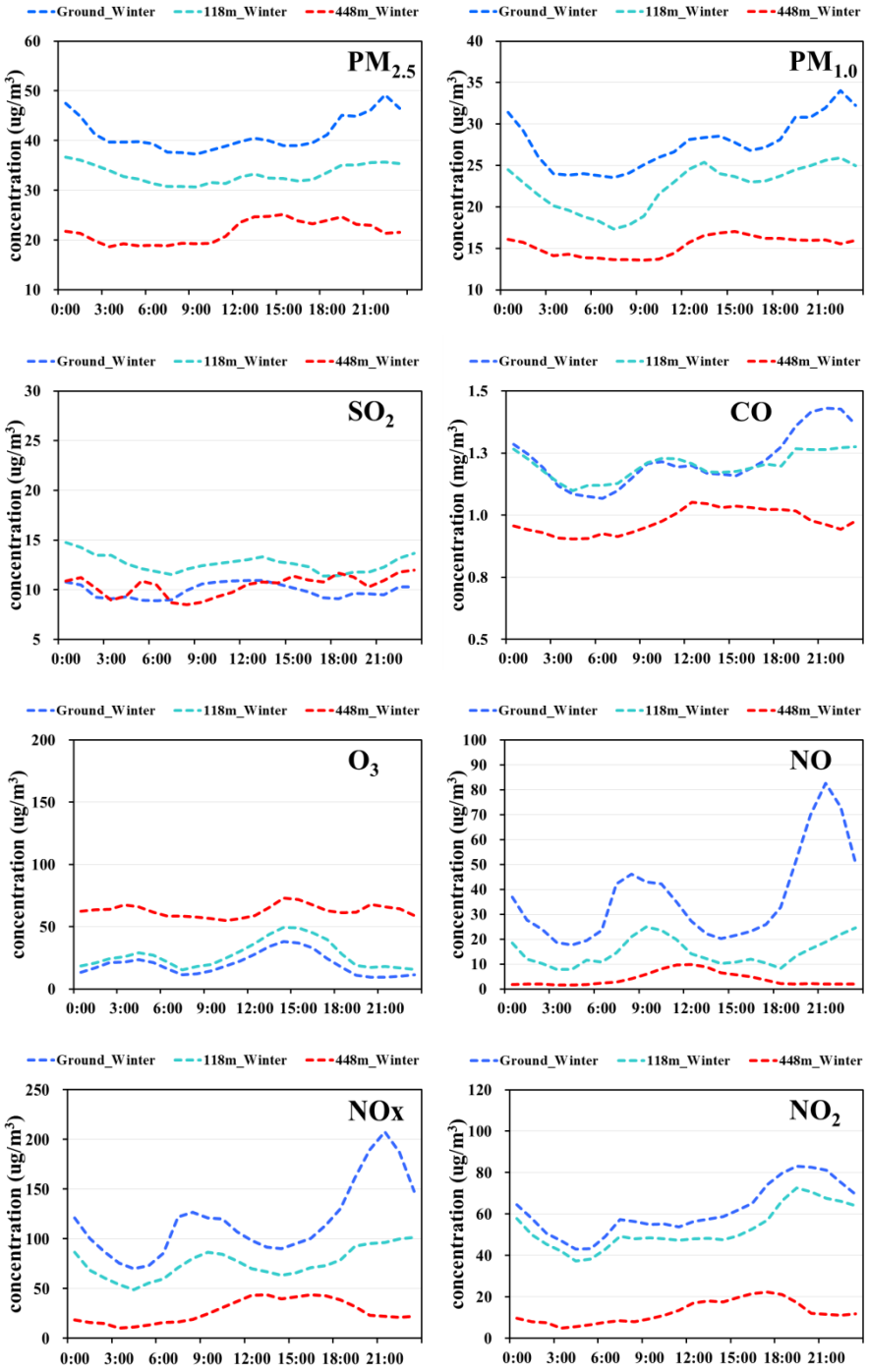

Figure S2. Diurnal variations of concentrations of pollutants at different altitudes on the Canton Tower during the winter field stuty.

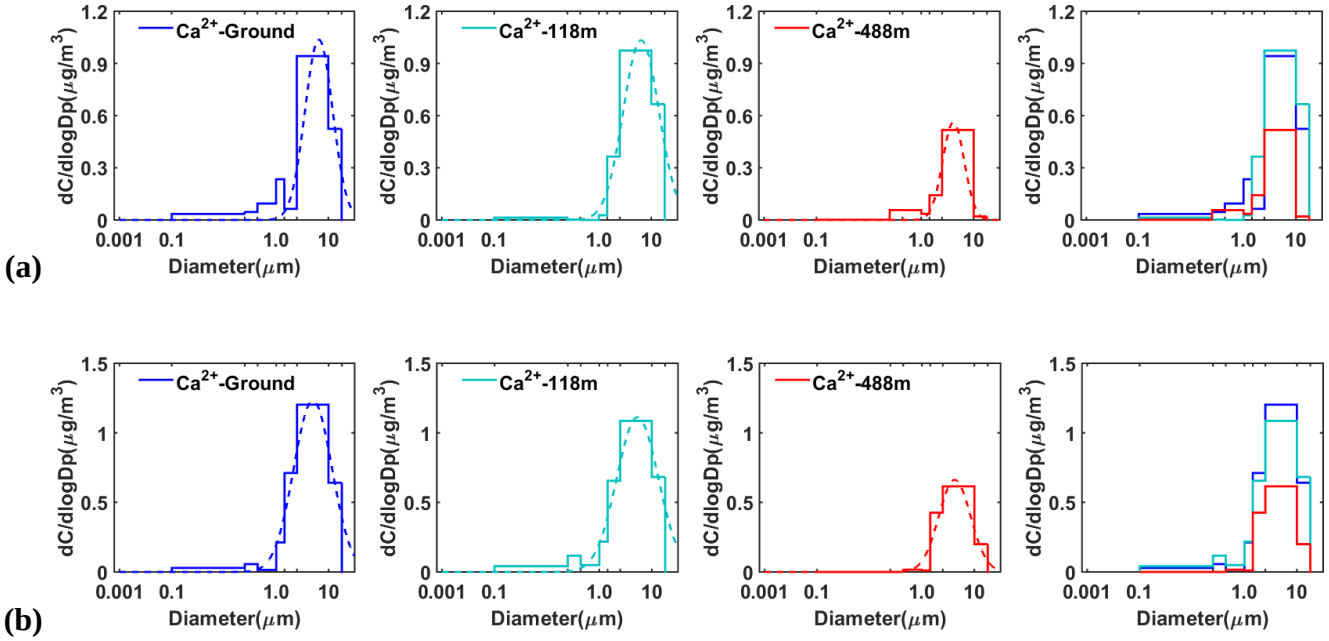

Figure S3. Mass concentration size distributions of Ca^{2+} measured at ground, 118 m and 488 m in winter: (a) autumn; (b) winter.

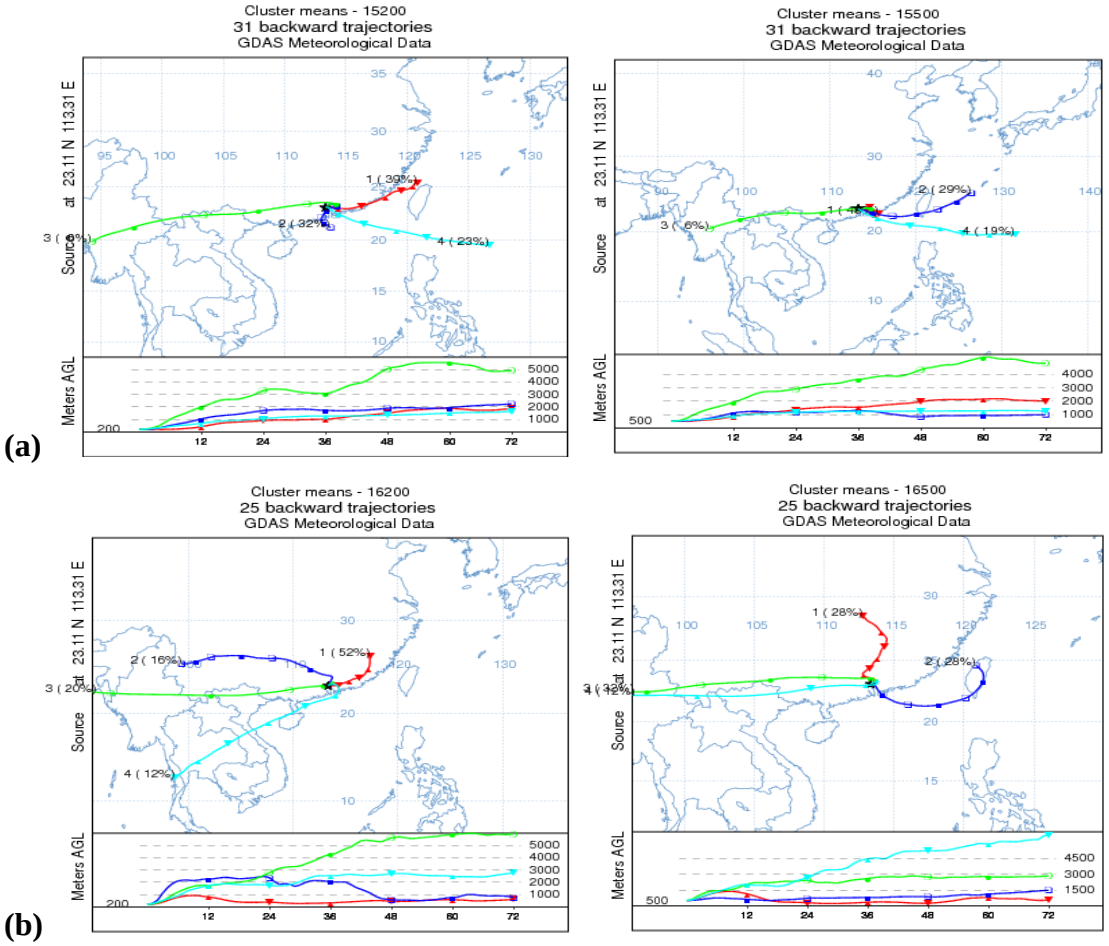

Figure S4. Cluster analysis of the airflow in 200 m and 500 m in (a) autumn and (b) winter campaigns.

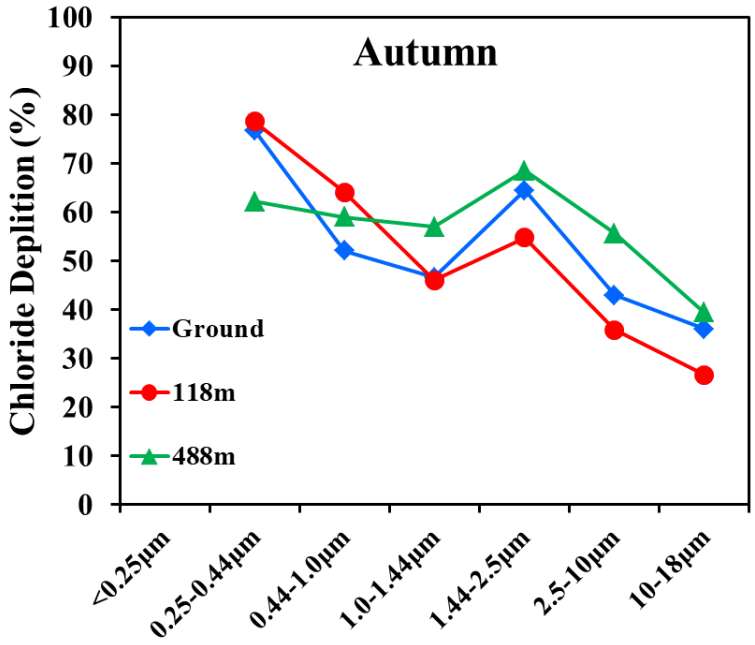

Figure S5. The percentage of chloride depletion at the three altitudes in autumn.

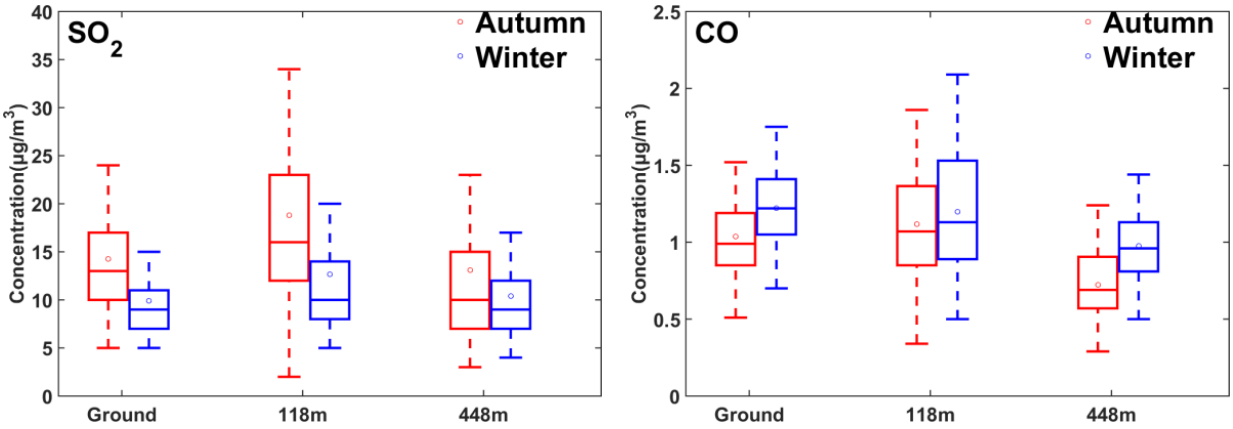

Figure S6. Concentration statistics of SO_2 and CO at different heights during the autumn and winter campaigns.

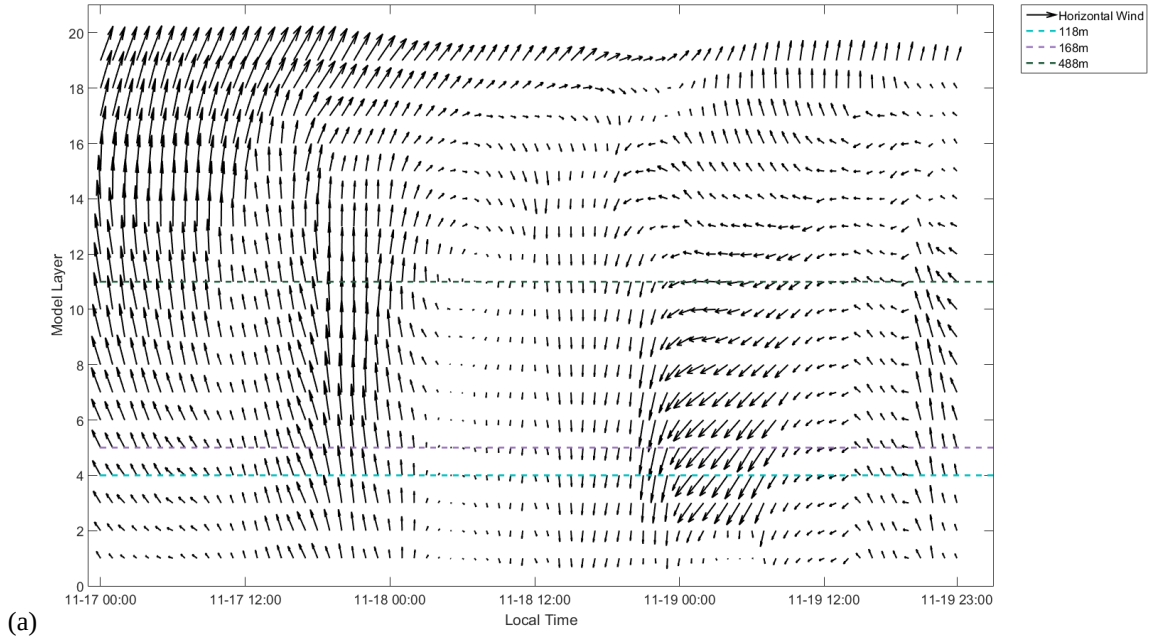

(a)

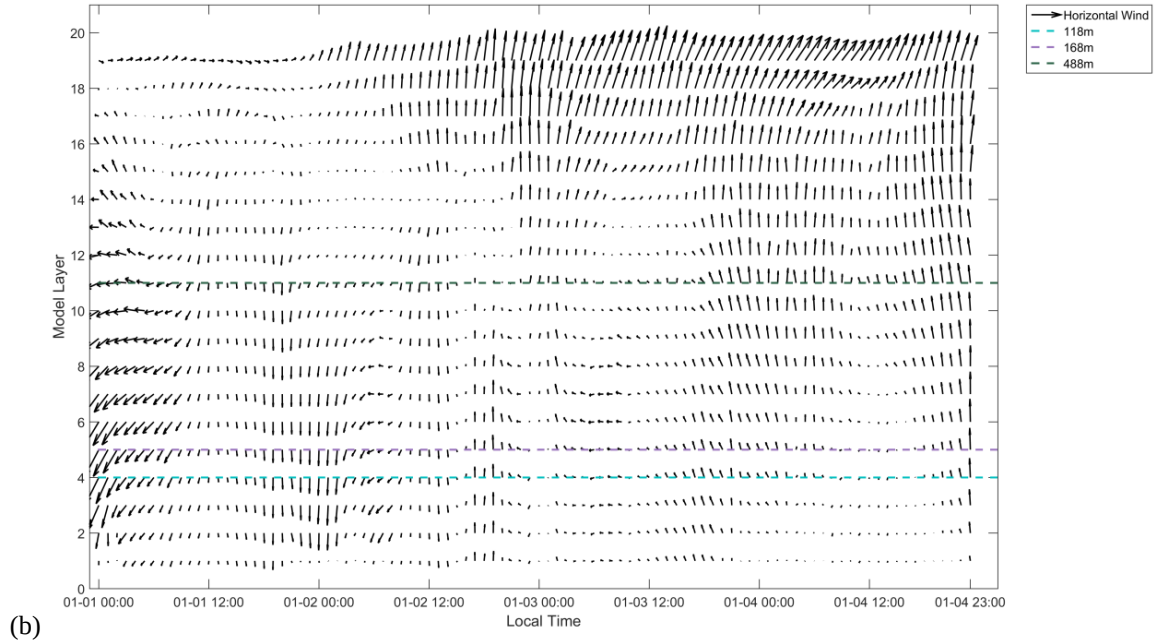

(b)

Figure S7. Modeled horizontal wind at different altitudes during (a) E1 episode in autumn; (b) E2 episode in winter.

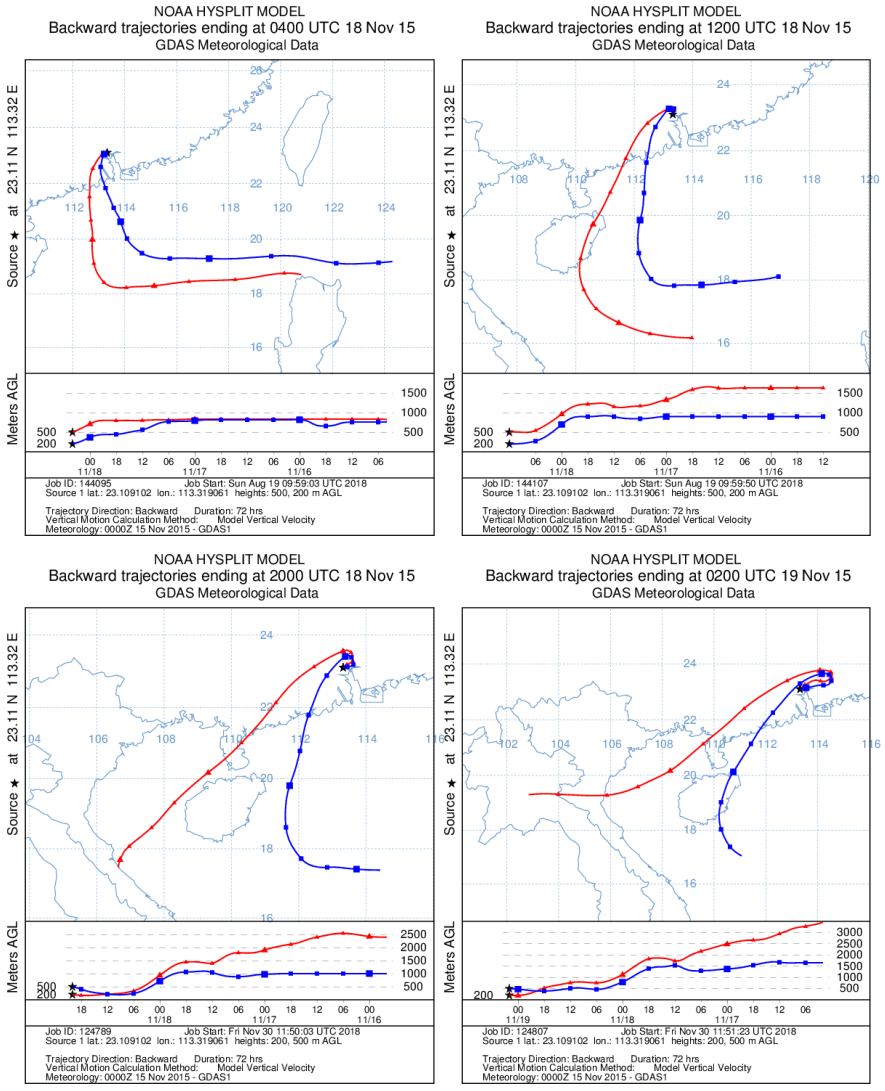

Figure S8. 72 h air mass back-trajectories analysis ending at the Canton Tower with height of 200 m and 500 m during E1 episode in autumn.

2. Weather Research and Forecasting (WRF) model setup and verification

2.1 Model Description and Configurations

Weather Research and Forecasting (WRF) model version 3.7.1(Skamarock et al. 2008) is adopted in this study. The WRF model is a new-generation mesoscale numerical atmospheric modeling system offering a host of options for atmospheric processes to serve both atmospheric research and operational forecasting needs. In the numerical modeling, a triple-nested grid with 27/9/3 km resolution domain and 39 layers in vertical is set (Figure S9). The simulation period is conducted from 0000 UTC 18 October to 0000 UTC 28 October 2015 as the autumn time period and 0000 UTC 25 December 2015 to 0000 UTC 28 January 2016 as the winter time period. The National Center for Environmental Protection (NCEP) 1 ° × 1 ° FNL (Final) operational global reanalysis data are applied as the initial and boundary condition in WRF modeling. The physical parameterization configurations for WRF model can be found in Table S2.

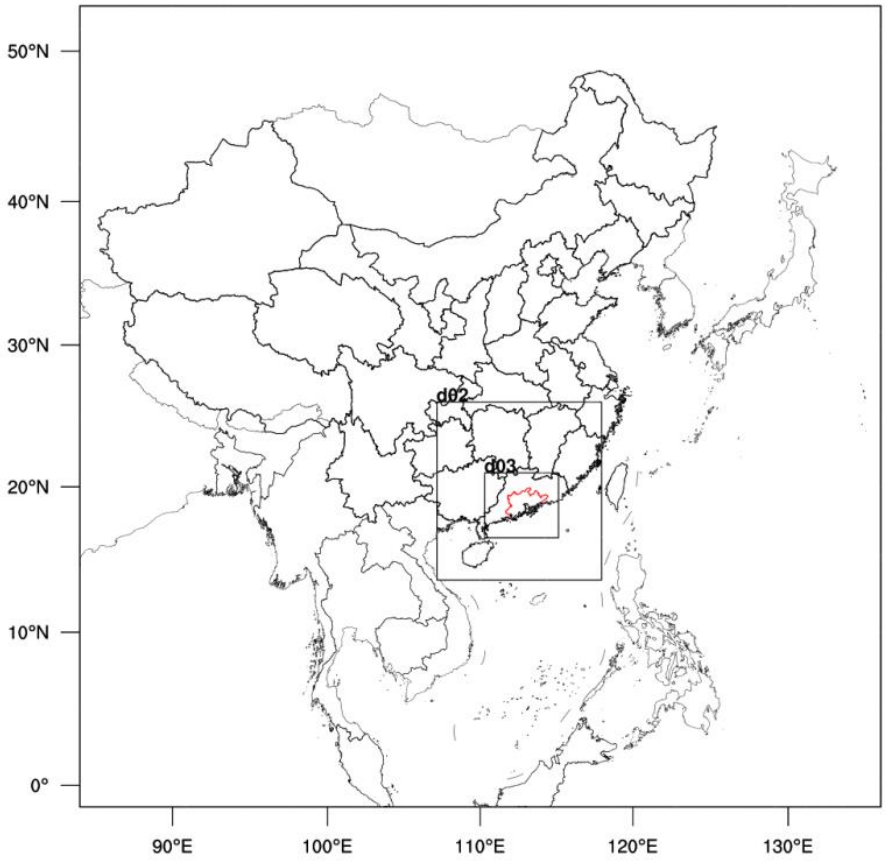

Figure S9. The triple-nested domain of WRF modeling.

Table S2. Physical parameterization configurations for WRF model

WRF v3.7.1	
Microphysics Scheme	Morrison (2 moments)
Cumulus Scheme	Kain-Fristsch
Longwave radiation Scheme	RRTM
Shortwave radiation Scheme	Dudhia
Boundary-layer Scheme	YSU
Land-surface Scheme	unified Noah
Urban Surface Scheme	UCM

2.2 Model validation and performance

The performance statistics for pressure, air temperature, relative humility and wind speed of three vertical layers on the Canton Tower are shown in Table S3. Here, the statistical measures such as Observation Mean, Simulation Mean, the Mean Bias (MB), the Normalized Mean Bias (NMB), the Normalized Mean Error (NME), the Mean Relative Bias (MRB), the Mean Relative Error (MRE), the Root Mean Squared Error (RMSE) and the correlation coefficient (CORR) are used for modeling validation.

Table S3. Comparison of Simulated Hourly Meteorological Variables with Observation Data

			Mean						
Meteorological Variables (Unit)	**Height**	**number[a]**	**Obs.**	**Sim.**	**MB**	**NMB[b]**	**NME[b]**	**RMSE**	**CORR**
Autumn									
PRES (hPa)	GND	925	1015.4	1013.8	-1.6	-0.2	0.2	1.8	0.98
	121m	950	1002.0	1002.1	0.2	0.0	0.1	0.7	0.97
	454m	952	959.9	959.3	-0.6	-0.1	0.1	1.2	0.94
TA (°C)	GND	952	24.8	24.2	-0.6	-2.6	5.5	1.7	0.92
	121m	950	23.4	23.2	-0.3	-1.1	4.2	1.3	0.94
	454m	952	20.6	20.8	0.2	0.7	4.0	1.1	0.95
RH (%)	GND	952	62.5	65.8	3.3	5.3	10.3	8.2	0.87
	121m	950	64.9	68.4	3.5	5.4	9.6	8.1	0.90
	454m	952	72.4	74.8	2.3	3.2	9.3	8.4	0.88
WS (m/s)	GND	952	0.7	2.5	1.8	250.3	253.7	2.1	0.66
	121m	753	2.1	5.0	2.9	138.3	141.6	3.7	0.39
	454m	936	4.1	6.1	2.0	47.6	58.7	3.2	0.66
Winter									
PRES (hPa)	GND	758	1021.2	1019.3	-1.9	-0.2	0.2	2.1	0.99
	121m	770	1006.8	1007.5	0.8	0.1	0.1	1.1	0.99
	454m	776	962.9	964.6	1.7	0.2	0.2	2.2	0.97
TA (°C)	GND	765	14.8	14.3	-0.5	-3.6	8.9	1.7	0.94
	121m	525	14.7	14.5	-0.2	-1.0	7.1	1.3	0.95
	454m	648	10.7	12.1	1.5	14.0	44.0	5.2	0.85
RH (%)	GND	765	67.0	69.5	2.5	3.7	10.1	8.8	0.86
	121m	522	82.2	74.4	-7.8	-9.5	10.5	11.2	0.88
	454m	245	73.9	60.7	-13.3	-18.0	23.1	19.8	0.88
WS (m/s)	GND	765	0.9	2.2	1.4	159.3	166.1	1.8	0.60
	121m	526	2.0	5.1	3.0	148.4	160.0	4.3	0.29
	454m	751	4.8	7.7	2.9	59.1	66.4	4.3	0.73

[a] the number of observed data

[b] the unit of NMB and NME is in %, other statistical variables are same as the meteorological variable

Reference:

Skamarock, W.C., et al., 2008. A Description of the Advanced Research WRF Version 3. NCAR Technical Notes, NCAR/TN-4751STR.